A&A 394, 1077–1091 (2002)
DOI: 10.1051/0004-6361:20021203

Astronomy & Astrophysics

Precise reduction of solar spectra obtained with large CCD arrays

H. Wöhl[1], A. Kučera[2], J. Rybák[2], and A. Hanslmeier[3]

[1] Kiepenheuer-Institut für Sonnenphysik, Schöneckstr. 6, 79104 Freiburg, Germany
[2] Astronomical Institute of the Slovak Academy of Sciences, 05960 Tatranská Lomnica, Slovakia
e-mail: akucera@ta3.sk; choc@ta3.sk
[3] Institut für Geophysik, Astrophysik und Meteorologie, Universitätsplatz 5, 8010 Graz, Austria
e-mail: arnold.hanslmeier@kfunigraz.ac.at

Received 3 December 2001 / Accepted 5 August 2002

Abstract. A precise procedure suitable for the reduction of solar spectra taken with large CCD arrays and the retrieval of correct spectral characteristics is presented. Various effects, which one should take into account, are considered and several improvements of the standard reduction are introduced. A special flat-field procedure is suggested for the reduction of spectra registered in different flat-field conditions than those when the flat-field matrix was taken. The original flat-field matrix is split into several components to eliminate the influence of the drift of the spectrograph and temporal changes of the flat-field conditions on the reduced spectrum. The importance of every flat-field matrix component is tested and discussed and the noise propagation through data reduction is analyzed. It is documented that the errors of the basic spectral line characteristics, continuum intensity, line centre intensity and full width at the half maxima of the line have variations between 0.5% and 15% and the errors of the line centre Doppler velocity and bisectors fluctuate by up to 200 m s^{-1}, if derived from imprecise reductions, compared to precise ones.

Key words. methods: data analysis – techniques: spectroscopic

1. Introduction

CCD detectors are widely used devices for the registration of photons. Their advantages compared to photographic film make this technique highly suitable for photometry and spectral analysis. Recent development of CCDs has increased significantly their geometrical dimensions. CCDs with chips of 1024 × 1024 pixels are widely used in solar and stellar astronomy. A few years ago, cameras with chips of 2048× 2048 pixels were put into operation for example at NSO, Sacramento Peak (see Kuhn et al. 1997) and at the German Vacuum Tower Telescope (VTT) operated by the Kiepenheuer-Institut für Sonnenphysik (KIS), Observatório del Teide, Tenerife (Kentischer & Schleicher 1997). New advanced computer technology, huge storage media capabilities and the high speed of data handling has brought the ability to take long time series of spectra with a high cadence of exposures. Several general guide books and articles appeared to help with reduction and restoration of the CCD spectra and images (e.g. Martines & Klotz 1998; Beletic & Amico 1998; Holst 1998; Newberry 1999). Nevertheless, any specific goal needs special arrangements for reductions which are not given in the references mentioned above. (See for example Harrison 1999, for flat-fielding of the solar long–slit spectra.)

Send offprint requests to: H. Wöhl,
e-mail: hw@kis.uni-freiburg.de

The aim of this paper is to introduce the reduction of solar CCD spectra taken with high spectral, spatial and time resolution, in long time series of several hours before and/or after the moment of the flat-field frames acquisitions. We will illustrate the whole process of reduction using solar high resolution 2D spectra taken with a large CCD detector.

The basic definitions are summarized in Sect. 2 and the observations are described in Sect. 3. We demonstrate the complete reduction process including an analysis of the spectrograph drift and the importance of different types of flat-fields in Sect. 4. Results are given in Sect. 5. The final discussion is presented in Sect. 6, where we compare and discuss the accuracy of three different types of reduction.

2. Basic definitions

The fundamental task of photometric spectrum reduction is to "clean" the observed raw spectrum without affecting the true spectral intensity information included in the image and to keep the S/N ratio as high as possible. It means that one must accurately account for the changes of intensities imposed by the imaging system. Under the term "imaging system" we consider here the optical system of the instrument as well as the CCD camera itself. The process by which a CCD image is adequately recovered is known as flat-fielding. Basically, the flat-field is a correction for the variation in response of the pixels in

Table 1. Main characteristics of KIS XEDAR CCD camera.

(1)	number of pixels: 2048*2048
(2)	mean pixel distance: 14 microns
(3)	vendor of the camera: XEDAR CORP., USA
(4)	chip used: Thomson TH/899M
(5)	sensitivity range: 400 nm to 1100 nm
(6)	window type: glass, wedge-shaped
(7)	interference pattern: not detectable
(8)	cooling: two stage cooling, at −10 deg C
(9)	controller: SUN workstation
(10)	digital precision: 12 bits

the image. If one took an image of a uniformly illuminated surface, then the ideal CCD image would show it as having constant counts in every pixel. The term "flat-field correction" then refers to the process of correction of the CCD image so that it acts as if it has uniform response everywhere. A flat frame is the 2D matrix used to make this correction. The basic flat-field correction can be described by the following equation:

$$R = \frac{(P - G)}{(F - G)/A}\,, \tag{1}$$

where R is the resulting reduced spectrum (image), P is the observed particular raw spectrum, F is the flat-field source frame, A is the average pixel value of the corrected flat-field source frame used for normalization, i.e. to scale the flat-field source frame to a mean intensity of 1.0 and

$$G = D + B + L \tag{2}$$

is the background composed of dark current D, bias B and scattered light L.

Although, the Eq. (1) seems to be very simple, doing flats is certainly complicated. Every term of the right side of the Eq. (1) exhibits difficulties in flat-fielding of real solar spectra observed with a real CCD camera. Generally, the background G can change during the observing run, the bias B is not constant with time or temperature and the scattered light L could change with a different setup of the instrument. The flat-field is used not only to take care of non–uniform response across the surface of the chip, but it is also used to take care of defects in the optical system that result in non–uniform illumination of the chip. These could be reflections, dust, shutter effect and any other non–uniformities, whatever their source. Therefore the flat-field is absolutely essential for precise photometric analysis of CCD spectra. Because there are many different factors that cause response variations, there are actually many different kinds of flat-field source frames to create and apply to an image. Therefore, a more general relation for n flat-fields takes the following form:

$$R = S \prod_{i=1}^{n} \frac{1}{M_i}\,, \tag{3}$$

where

$$S = P - G \tag{4}$$

is the spectrum from which the background G was subtracted and

$$M_i = \frac{F_i - G}{A_i}\,, \quad i = 1, 2, ...n, \tag{5}$$

where F_i are flat-field source frames used for every ith particular effect of non-uniform response of the chip or non-uniform illumination of the chip. The common types of flat-fields we will deal with in this paper are:

M_1 – "pixel-flat": the flat-field used for correction of the non–uniform sensitivity of the pixels across the chip; This is generally wavelength dependent. But in the case of high spectral resolution CCD spectra only a very short range in wavelength (∼3 Å) is taken on the chip, so the effect is negligible in our case;

M_2 – "illumination-flat": the flat-field which will correct large gliding changes of the intensity across the chip caused by optical vignetting, dust particles imaged out of the focus, etc.

M_3 – "shutter-flat": flat-field used to suppress the non-uniformity of the exposure caused by the finite travel time of the shutter across the field of view;

M_4 – "camera-flat": flat-field for correction of CCD camera effects, for example interference at the glass window of the CCD camera or dust lying on the CCD camera window. Generally, the interference is wavelength dependent and also the introducing of any optical filter on the camera window changes this flat-field matrix;

M_5 – "slit-flat": flat-field for corrections of the non-uniform illumination of the chip caused by the dust lying on the spectrograph slit and/or by imperfection of the slit and/or by non-parallel edges of the slit;

M_6 – "segment-flat": flat-field for corrections of the different sensitivity of sub-chips to light. (The CCD detector we used is composed of four independent segments).

Sometimes several types of flat-fields must be grouped into one flat-field matrix M for correction of several effects together. We will show later that in the case of large solar spectra all the flat-fields must be derived from one flat-field frame.

3. Observations

We will demonstrate the full procedures of precise reduction of CCD spectra and spectral line characteristics determination using spectra taken at the VTT with an echelle spectrograph described by Schröter et al. (1985). The observations were performed at the VTT on April 28, 2000 with two 2048 × 2048 XEDAR CCD cameras (see Table 1). The observing project included observations in two spectral regions simultaneously. The spectra were exposed with a high cadence of 3 s for several hours. Here, we will deal with the observations of the spectral range (roughly ∼3 Å wide), centred on the Fe II 6456.396 Å line.

A quiet area near the solar disc centre was observed. More than 1000 exposures of spectra, flat-field source frames and background frames were collected. The width of the entrance slit of the spectrograph was 100 μm. The exposure time of every particular raw spectrum P as well as of the flat-field source frame F and background frame G was 1.0 s. The binning mode

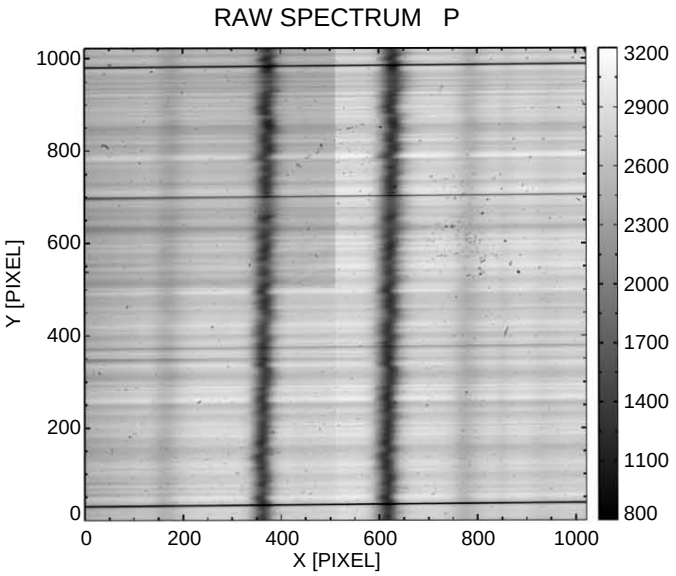

Fig. 1. The particular raw spectrum P as observed with a large CCD camera at VTT, Tenerife. The grey-scale bar gives relative intensities expressed in ADU (Analog-Digital Units).

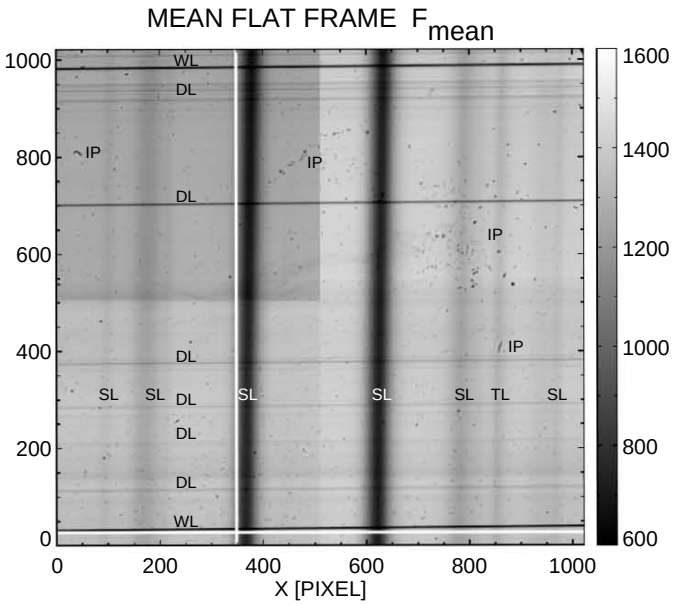

Fig. 2. The mean flat-field frame F_{mean} as constructed using Eq. (9) with $K = 40$. WL = pictures of the artificial wires put on the spectrograph slit; SL = spectral lines; TL = terrestrial spectral line; DL = "dust" lines caused by dust particles lying on the slit; IP = imperfections coming mainly from invalid pixels of the CCD chip. Inclination and stretching of the spectral line(s) and inclination of the horizontal wires are pointed out by the white vertical and horizontal lines, respectively. Different sensitivities of the four segments of the chip are obvious. The grey-scale bar gives relative intensities expressed in ADU.

was switched to 2×2, it means that the final spectrum has 1024 pixels in both the wavelength and spatial directions. The line Fe II 6456.396 Å was observed in the 35th order. Thus, one pixel corresponds to 3.097 mÅ in the wavelength direction and one spatial step corresponds to 0.125 arcsec.

The typical CCD raw spectrum P taken at the spectrograph of the VTT using the large CCD camera is shown in Fig. 1, where X denotes the wavelength direction and Y denotes the space direction along the spectrograph slit.

4. Reduction of spectra

We describe in detail all the steps (sometimes rather trivial) of the reduction process to keep an instructive scheme of the whole one. Spectral characteristics at three different steps of the reduction process were retrieved to demonstrate an increase in the precision of the results by using more precise steps of reduction.

The *precise* reduction process consists of:

- 1. subtraction of the background G from the particular raw spectrum P;
- 2. construction of the mean flat-field frame F_{mean};
- 3. extraction of the segment-flat M_6 from the mean flat-field frame F_{mean};
- 4. retrieving of the components $M_{1,2,3,4,5}$ from the mean flat-field frame F_{mean};
- 4.1 precise restoration of the X inclination of the image;
- 4.2 de-stretching – the restoration of the curvature and Y inclination of the spectral line;
- 4.3 construction of the flat-field matrix M;
- 4.4 extracting the slit-flat M_5 from the flat-field matrix M;
- 4.5 shift of the slit-flat M_5;
- 5. flat-fielding.

In the *simple* approach of the flat-fielding we omitted the steps 4.1, 4.2, 4.4, and 4.5. This means that the flat-fielding was done with the flat-field matrix M which was constructed directly from the raw mean flat-field frame F_{mean} (cf. Fig. 2) corrected for the segment-flat M_6.

In the *extended* approach of the flat-fielding we omitted step 4.5. The consequence is that the flat-field matrix M is shifted compared to the spectrum S.

The reduction was performed with programs written in the Interactive Data Language (IDL) using also the IDL KIS package at the Kiepenheuer-Institut für Sonnenphysik, Freiburg.

4.1. Subtraction of the background G from the particular raw spectrum P

In real spectra, the background G given in the Eqs. (1), (2), (4) and (5) consists of the noise of the CCD camera (dark current D), of the bias B, introduced by the readout electronics of the CCD and of the scattered light L coming from the spectrograph with a closed shutter. As was mentioned in Sect. 2, the background G can vary during the observation. The bias B varies with temperature, so the best way to keep it constant is to use the cooling control of the CCD camera. If this is not the case, one must estimate the sensitivity of the bias B to the temperature changes experimentally and then use an appropriate background G image according to the actual temperature during the acquisition of the spectra. Measurement of the background G should also be repeated if any change of the setup of

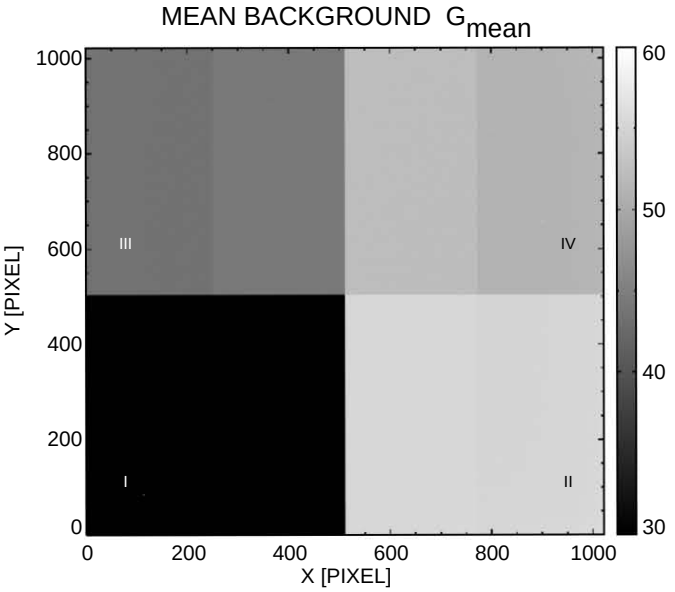

Fig. 3. Average background $G_{\rm mean}$ belonging to the spectra in Figs. 1 and 2. The grey-scale bar gives relative intensities expressed in ADU. Segment numbers are denoted inside the figure.

the instrument was done concerning the change of the scattered light in the instrument.

To keep the S/N ratio as high as possible it is useful to average several background G frames (see Newberry 1991, for a more detailed description of signal-to noise considerations).

Thus, the Eq. (4) takes the following form:

$$S = P - G_{\rm mean}\,, \tag{6}$$

where

$$G_{\rm mean} = \frac{\sum_{j=1}^{J} G_j}{J} \tag{7}$$

is the average of several particular background images G including the dark current D, bias B and scattered light L. The background G was stable during the whole observation run because the CCD camera was equipped with a cooling control. Therefore we used the average of the first 7 background images G for corrections. An example of $G_{\rm mean}$ is demonstrated in Fig. 3. The mean value of the intensity of the $G_{\rm mean}$ was 44.96 ADU. 100 ADU was automatically added to every background frame (as well as to all other frames) to avoid negative values. The segments I, II, III and IV, denoted in Fig. 3, had relative intensities to the mean 0.636, 1.227, 0.978 and 1.150, respectively. Different intensities of the segments are due to different bias, i.e. due to nonuniform readout of the electronics of the four segments. Each particular raw spectrum P as well as flat-field source frame F was corrected for $G_{\rm mean}$.

4.2. Construction of the mean flat-field frame F_{mean}

In this section we will deal with the difficulties of taking flat field source frames F and mean flat-field frame $F_{\rm mean}$ that serve as the basis for the computation of the flat-field matrix M. We will focus on the special case of a solar spectra taken with a large CCD array.

As we stated in Sect. 2, the flat-field is used to correct both the non-uniform response across the surface of the chip and non-uniform illumination of the chip. Therefore, it is not enough to illuminate the chip with uniform light and use the resultant exposure for correction. The uniform light must pass through the complete optical system with an identical focus, exposure time and other conditions as those valid for every particular spectrum P. Moreover, the spectral range of the flat-field source frame F should match that of the object being imaged. Therefore, for solar CCD spectroscopy, the ideal source for flat-fielding should be at infinity, should be a source similar to sunlight and the light must pass through the telescope and spectrograph. From these last requirements it is clear that it is impossible to get ideal artificial uniform light from infinity for flat-fielding in this case and the Sun itself is the only source intensive enough to mimic observational conditions. Thus, the flat-field source frames F must be derived from images that are almost identical to the particular raw spectrum P. There are several ways to create the flat-field source frames F in this case:
a) the simplest way is to sandwich all particular raw P images we made and get an average "soft" spectrum with smoothed spectral line(s);
b) the second possibility is to de-focus the telescope and to make enough un-sharp images. Then we construct the average of them to obtain a similar result to the previous case;
c) The third method of creation of the flat-field source frame F is to move the image of the Sun across the slit in the focal plane of the telescope and take a lot of images. The average of such images will give a similar result to the previous two cases, because the spectral lines will be smeared due to the fast movement of the solar image across the spectrograph slit. It is also possible to use a combination of the second and third methods (e.g. Johannesson et al. 1992).

It is useful to take the flat-field source frames F very often, to minimize the influence of the temporal changes of the flat-field conditions. Many cases of observations do not allow us to make flat-field source frames F very often. For example, the simultaneous observations with VTT and space instruments or investigation of temporal changes in the solar atmosphere require uninterrupted long series of observations. Then, one can take the flat-field source frames F only at the beginning and at the end of the observing run. So the temporal changes of the flat-field conditions introduce rather serious problems for the reduction of these spectra.

It is clearly seen, from the methods mentioned above, that all non-uniform illuminations of the chip in the case of large solar spectra are grouped together into one mean flat-field frame $F_{\rm mean}$. Namely, the $F_{\rm mean}$ for the first (sandwiching) method will be defined as:

$$F_{\rm mean} = \frac{\sum_{k=1}^{K}[P_k - G_{\rm mean}]}{K}, \tag{8}$$

where K is the number of all particular raw spectra P and $G_{\rm mean}$ is the mean background. For the second and third methods the $F_{\rm mean}$ is given by:

$$F_{\rm mean} = \frac{\sum_{k=1}^{K}[F_k - G_{\rm mean}]}{K}, \tag{9}$$

where K is the number of the flat-field source frames F taken with de-focused telescope and/or with moving solar image across the focal plane of the telescope.

However, all three methods for the construction of $F_{\rm mean}$ have some limitations. Usually, one tries to observe the long series during the best seeing conditions, keeping the spectrograph slit in the same position of the solar disk or scanning within small areas. Thus, the average of many raw spectra P still exhibits shifted patterns which remain from the real Doppler velocity shifts of a particular part of every particular raw spectrum P. This results in non-uniform $F_{\rm mean}$ in the case of the first method. The second method with the de-focused telescope tends to optically disturb the spectrum giving rise to lateral displacement of the location of the spectral line(s) in the image plane in the camera and changes the fixed pattern, particularly the variations due to fringing and illumination. A similar displacement of the spectral lines could appear when one moves the telescope, if the scanned area at the solar disc is very large. This smears the spectral line due to averaging of shifted lines caused by real differential rotation of the Sun.

We used the third method for construction of the mean flat-field frame $F_{\rm mean}$. The quick movement of the telescope was kept very near to the disc centre in a quiet region to minimize the mentioned above displacement effects in every particular flat-field source frame F. The final $F_{\rm mean}$ was an average of 40 particular flat-field source frames F from which $G_{\rm mean}$ had previously been subtracted. The mean flat-field frame $F_{\rm mean}$ is given in Fig. 2 with a description of the most important features in the spectrum. Identical features also appear in the raw spectrum P shown in Fig. 1.

The $F_{\rm mean}$ contains all six flat-fields M_i mentioned in Sect. 2, and also the spectral lines as a consequence of the facts discussed in the beginning of this section. In the following sections we show how to retrieve the particular M_i from the mean flat-field frame $F_{\rm mean}$.

4.3. Extraction of the segment-flat M_6 from the mean flat-field frame F_{mean}

The chip is composed of four independent parts which differ in sensitivity. Therefore, the segment-flat M_6 that bears only this differences is not affected by the presence of the spectral lines in the mean flat-field frame $F_{\rm mean}$. So, it is possible and useful to extract the M_6 from the mean flat-field frame $F_{\rm mean}$ before further image manipulation. In addition, the segment-flat M_6 has fixed geometrical, rectangular stability and further manipulations of the mean flat-field frame $F_{\rm mean}$, which are described in the following subsections, would change the geometry of the segments. On the other hand, if the mean flat-field frame $F_{\rm mean}$ were not corrected for the segment-flat M_6 before applying of the smoothing procedures required for rubbing out the spectral lines, the different intensities of the segments of the flat-field frame $F_{\rm mean}$ would affect the smoothing procedure.

In fact the four segments of the CCD chip also differ in the bias B, but this was already compensated for in Sect. 4.1.

Because the flat-field M_6 is uniform within every subsegment, it is enough to estimate the ratios of sensitivities between them and simply construct the segment-flat matrix M_6 as a matrix of four subsegments with appropriate ratios of sensitivities between them. We experimentally determined the sensitivities of the segments which are equal to 1.004, 1.029, 0.930 and 1.037 for segment I, II, III and IV, respectively, comparing to the mean intensity of the whole chip, normalized to unity. The designation of the segments is identical as in Fig. 3. We have found the stability of the sensitivity of the individual segments to be within the range of ±0.1% for the intensity range of 400–3200 ADU. Obtaining the segment-flat M_6, it was possible to correct the mean flat-field frame $F_{\rm mean}$ by dividing it by M_6. Logically, the spectrum S was also corrected in the same way at this stage of the reduction process. We will name this improved spectrum S_1. It will be used in the *simple* reduction approach.

4.4. Retrieving of the flat-field matrix ($M_{1,2,3,4,5}$) from the F_{mean}

First, several manipulations with the mean flat-field frame $F_{\rm mean}$ will be done in this section, to prepare it for a correct derivation of the flat-field matrices. Then, we will define the flat-field matrix M which is composed of five ($M_{1,2,3,4,5}$) components. The elimination of the spectral lines from the flat-field matrix M will be described and finally each particular flat-field matrix will be extracted from the mean flat-field frame $F_{\rm mean}$.

It was possible to extract the segment-flat M_6 from the mean flat-field frame $F_{\rm mean}$ even when the spectral lines were presented. This is not the case in the other flat-field matrices. The spectral lines constrain the flat-field matrices and we must erase them from the $F_{\rm mean}$. The smoothing processes used for retrieving the flat-field matrix M are applied to spectra in both the X and Y directions in the image. To run them correctly it is necessary to have the mean flat-field frame $F_{\rm mean}$ (as well as the spectrum S_1) parallel to both edges of the CCD camera.

4.4.1. Precise restoration of the X inclination of the image

The horizontal sharp lines in the particular raw spectrum P as well as in the mean flat-field frame $F_{\rm mean}$ (see the inclined WL and DL in Figs. 1 and 2) are artificial and/or natural. The artificial horizontal lines (WL) are images of wires placed on the spectrograph slit to adjust spectra taken by different CCD cameras in different spectral regions. The natural horizontal lines in the spectrum come from defects of the spectrograph slit. These defects are caused by dust particles on the slit of the spectrograph (DL – dark lines – less intensive) and by holes in the sharp edges of the slit (bright lines – more intensive). One should try to adjust the CCD camera in the focal plane of the spectrograph to align the edge of the image (the X axis) parallel to the horizontal sharp lines appearing in the spectrum. In any case, some inaccuracy (even a fraction of pixel) remains. This introduces problems in the next steps of reduction and also if one tries to calculate continua on the left and right side of a spectral profile using one row of the spectrum. To make the

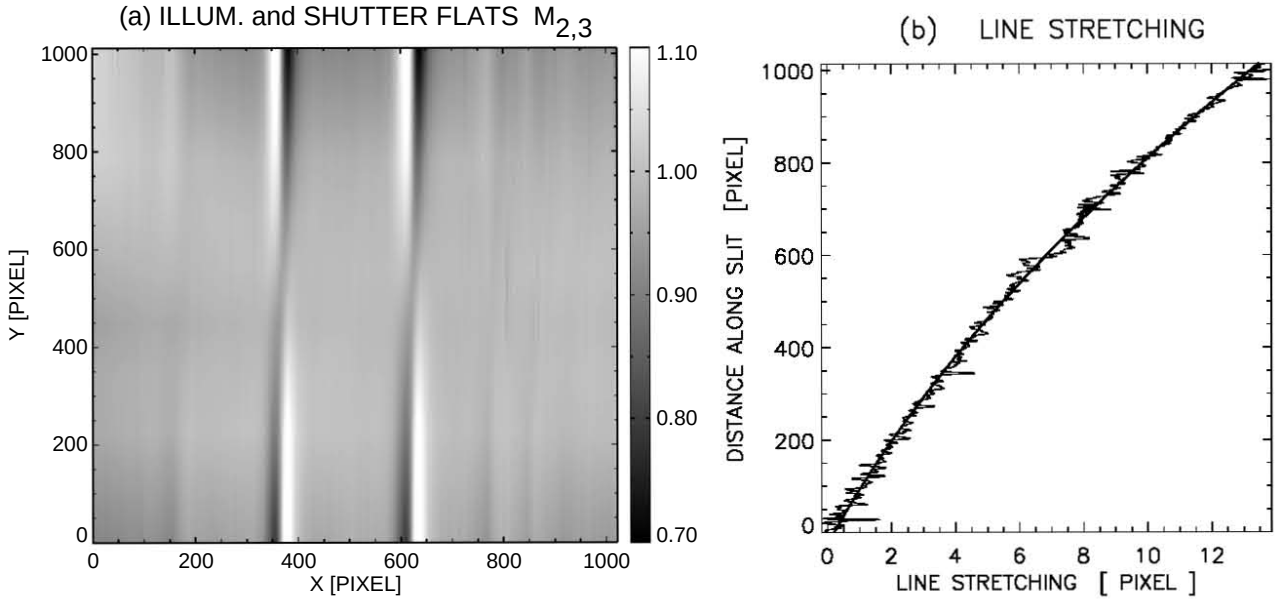

Fig. 4. a) An incorrect flat-field matrix $M_{2,3}$ composed of the illumination-flat and the shutter-flat as a resultant from the mean flat-field frame F_{mean} which was not corrected for stretching and inclination of the spectral lines. The grey-scale bar gives relative intensities normalized to 1; **b)** The stretching and inclination of the spectral lines determined in Sect. 4.4.2. Fluctuations of the centres of the spectral profiles along the spectrograph slit are shown by the thin line and the polynomial approximation is represented by the thick line.

horizontal lines parallel to the edge of the image we used our procedure which allows us to shift the columns of the CCD image in the Y direction gradually with an arbitrary predefined accuracy without shifting of any part of the spectrum in the X direction. Re-binning and shifting of every particular column of the image in the Y direction with an accuracy of 1/100 of a pixel was performed in this particular reduction. As a consequence of our approach several incomplete rows at the top or at the bottom of the image had to be cut away. This didn't affect the next steps of the reduction, because only pure spectra between the two WL wires were finally used for calculations of spectral characteristics. The shifts were applied to both the mean flat-field frame F_{mean} and the spectrum S_1.

4.4.2. De-stretching – restoration of the curvature and Y inclination of the spectral line

The spectral lines in both the spectrum S and the mean flat-field frame F_{mean} exhibit curvature and inclination along the slit (along Y). The curvature is caused by the spectrograph design and the line inclination appears due to an inaccuracy in the adjustment of the parallel between the vertical edges of the CCD camera and the spectrum.

The correction of spectral line stretching and inclination is essential for the next steps of flat-fielding. To erase the spectral line from the F_{mean} the smoothing also runs in the Y direction in the image. If the spectral line in the F_{mean} is not strictly vertical, i.e. parallel with the Y edge of the image, the process will not work correctly, as we will see later. The best procedure to estimate line "stretching" is to utilize a terrestrial line if it is available in the spectrum. Such a line has a well defined and stable centre. The positions of the centres determined for every scan directly reflect the curvatures and inclination of the spectral lines in the particular spectral region. But often there are no terrestrial lines available in the spectrum or the terrestrial lines are very weak, e.g. as in our case. Here we used the smoothed observed line itself derived from the mean flat-field frame F_{mean} as the source of the required information. Again, the vector of the positions of the centres of the particular line profile (row) gave us information about the curvature and inclination of the spectral lines along the slit. Such a vector is given in Fig. 4b. The vector of the positions of the centres was approximated by a polynomial approximation of the second order in this case (thick line in Fig. 4b). The resulting polynomial approximation was finally used for shifts of every particular scan (row) in the X direction to make the spectral lines parallel to the Y edges of the image. An identical polynomial approximation for shift was applied to both the mean flat-field frame F_{mean} and the spectrum S_1. This again, similar to the previous step, required several incomplete columns on the left and right of the image to be cut away. The prepared spectrum S_2 and the mean flat-field frame F_{mean} after all steps of the reduction mentioned above are shown in Fig. 5. The spectrum S_2 will be used in the *extended* and *precise* reduction.

4.4.3. Construction of the flat-field matrix M

The flat-field matrix $M_{1,2,3,4,5}$ will be defined in our case formally with an equation similar to the Eq. (5) which defined the ith particular flat-field matrix M_i but our resulting matrix M will be composed of five flat-fields and it will still contain the spectral lines. These lines must be erased from the matrix M to get the flat-field frame(s) commonly used for flat-fielding. The flat-field matrix equation reads:

$$M = \prod_i M_i = \frac{F_{\text{mean}}}{A}, \quad i = 1, 2, ..5 \tag{10}$$

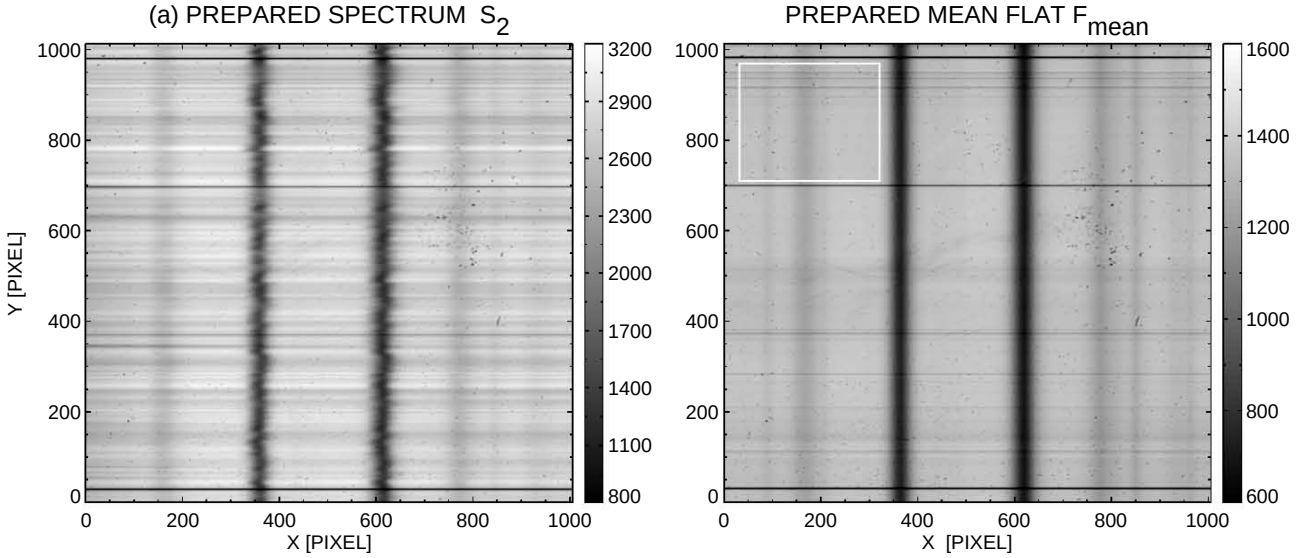

Fig. 5. The prepared spectrum S_2 **a)** and the prepared mean flat-field frame F_{mean} **b)** after corrections for segment-flat M_6, for X inclination and for stretching and Y inclination of the spectral lines. The grey-scale bars give relative intensities expressed in ADU. The rectangular box marked the area where the standard deviations were calculated (see Sect. 5).

where M is the flat-field matrix composed of the five individual flat-field matrices and of spectral lines, A is the average pixel value used for normalization and F_{mean} represents the mean-flat field frame defined by Eq. (9). Different F_{mean} were used for different approaches of the reduction. The F_{mean} created from the raw mean flat-field (Fig. 2) and corrected for segment flat M_6 was used in the *simple* reduction. The manipulated F_{mean} shown in Fig. 5b was used in the *extended* and *precise* reduction.

Equation (10) is calculated in two steps:

- The flat-field matrix composed of the illumination-flat M_2, of the shutter-flat M_3 and of spectral lines is derived from F_{mean}. This we call a "soft", part of the flat-field matrix M due to its smooth character;
- The flat-field matrix composed of the pixel-flat M_1, the camera-flat M_4, and the slit-flat M_5 is retrieved from F_{mean}. This we call a "hard" part of the flat-field matrix M due to its sharp "spiky" character.

The procedure smooths the image with a rectangular box (window) in both directions. Then additional smoothing of scans (rows) in the X direction by a least squares function spline is done and finally, for each column of the image the linear interpolation along the Y direction between the scans of the predefined box (window) is carried out. We used a window of 9 pixels width.

Dividing the mean-flat field frame F_{mean} by the "soft" part of the flat-field matrix M we derived the "hard" part of the flat-field matrix M. This is shown in Fig. 6a. Then the spectral lines are eliminated from the "soft" part of the flat-field matrix M dividing this part by "mean scan". It is constructed as an average of all rows of the image. From this last step it is clear why the spectral lines must be parallel to the Y edge of the image. If it is not the case, some residual intensities in every row of the image will remain. This incorrect resulting "soft" flat-field matrix $M_{2,3}$ is shown in Fig. 4a. The correct "soft" $M_{2,3}$ is shown in Fig. 6b.

4.4.4. Extracting the slit-flat M_5 from the "hard" part of the flat-field matrix M

In this section, we will first analyze the main reason for the temporal changes of the flat-field conditions, the spectrograph drift. Then we will show that the time dependent parts of the flat-field matrix M are the slit-flat M_5, and illumination-flat M_2. Finally we will demonstrate how to solve post factum the problem of the temporal changes of the flat-field conditions. We split the "hard" part of the flat-field matrix M into two components, the slit-flat M_5 and the flat-field matrix $M_{1,4}$ composed of pixel-flat and camera-flat.

Drift of the spectrograph

Spectrographs with high resolution and dispersion exhibit drift of the spectral lines and changes of the dispersion, e.g. due to thermal bending of mechanical components, like support structures of the slit basement, the collimating and focusing mirrors and the grating itself. It has to be taken into account that asymmetric heating of the solar towers occurs in the daytime with sunshine coming in the morning from the east and in the afternoon from the west. This can be measured with terrestrial spectral lines (e.g. of oxygen), laboratory molecular lines (e.g. of iodine) or laser reference lines. A detailed investigation made by Thiele (1982) showed for the solar spectrograph at Locarno drifts up to 0.5 pm per hour. Such drifts can still be determined using terrestrial oxygen lines. There was a high correlation of the drifts and changes of their sign with the recorded temperature in the environment in the data of Thiele. Very stable lasers used to control a Fourier Spectrometer (Brault 1979) allowed the determination of even

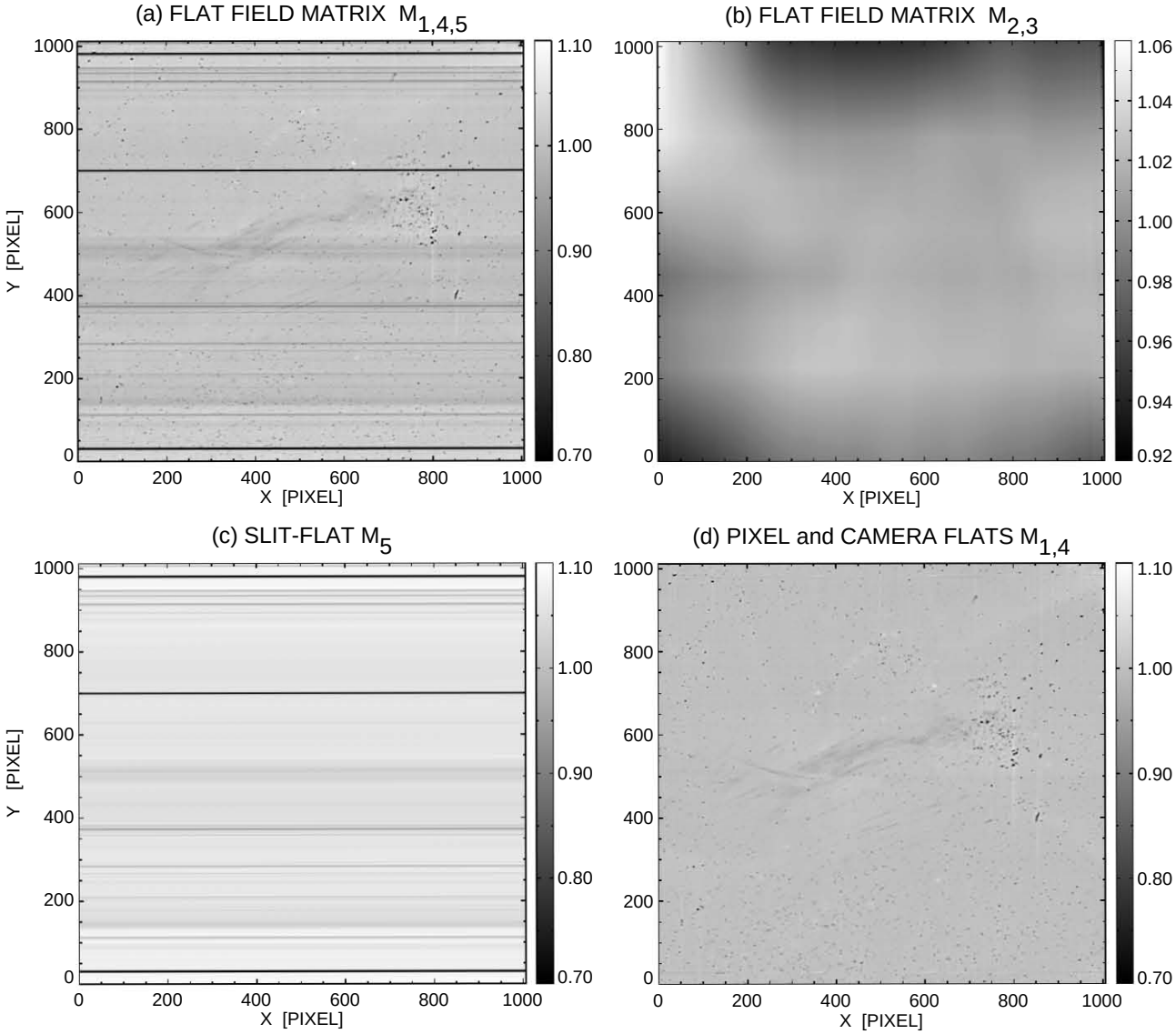

Fig. 6. a) The "hard" flat-field matrix $M_{1,4,5}$ composed of the pixel-flat, the slit-flat and the camera-flat; **b)** The "soft" flat-field matrix $M_{2,3}$ composed of the illumination-flat and shutter-flat; **c)** The slit-flat matrix M_5; **d)** The flat-field matrix $M_{1,4}$ composed of the pixel-flat and camera-flat. The grey-scale bars give relative intensities normalized to 1.0.

shifts of the oxygen lines of the order of 0.01 pm within a day due to wind in the Earth's atmosphere (Balthasar et al. 1982).

For the VTT no published data about the drift of its spectrograph exist. Within the investigation performed in 1988 one of the authors (H.W.) determined drifts using terrestrial oxygen lines 6302.005 Å and 6302.771 Å. He found drifts that ranged from 0.015 pm within a minute up to 0.3 pm within an hour in August 1988.

We also found the drift of the spectrum in the focal plane of the spectrograph of VTT in both directions in a data set observed in 1996 using different CCD cameras. Again the terrestrial lines of the oxygen molecule 6302.005 Å and 6302.771 Å were used for determination of the drift in wavelength direction. The wires (WL) in the images were used as tracers for determination of the drift in spatial direction. Values of 1.06 pm (1.3 pixel) per hour and 0.26 arcsec (1.5 pixel) per hour were found for the X and Y directions, respectively. In addition we have found that the drift was not linear. It was steepest in the morning and gradually decreased in the middle of the day.

The analysis of the drift made with the data used in this work shows that the drift in the spatial direction (the WL wires were used for tracking) was 1.7 pixel per hour that corresponds to 0.21 arcsec. It is in agreement with the previous results.

Time dependent parts of the flat-field matrix M

As we have documented above the spectrograph drift moves the image (spectrum) in the focal plane of the spectrograph in both the X and Y directions. This will affect only two components of the whole flat-field matrix M, namely the illumination-flat M_2 and the slit-flat M_5, because the other three $M_{1,3,4}$, i.e. the pixel-flat, the shutter-flat and the camera-flat are closely connected to the CCD camera body.

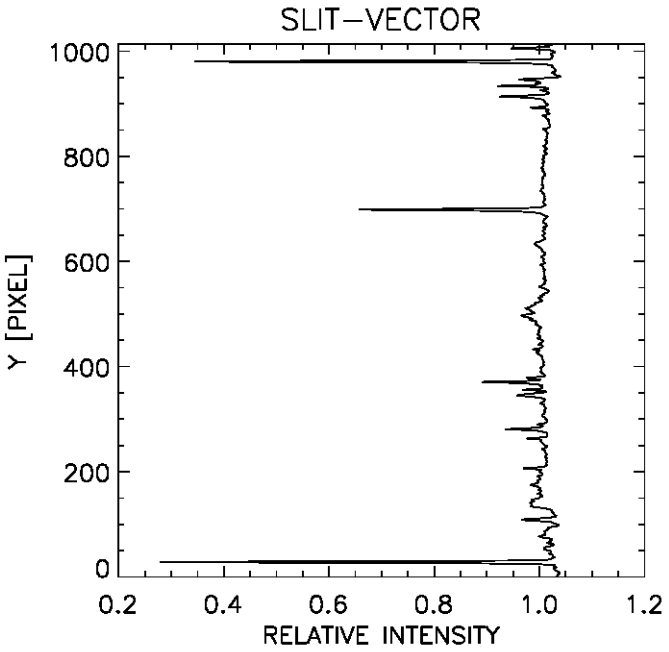

Fig. 7. The "slit-vector" which represents the average of all columns of the flat-field matrix $M_{1,4,5}$ shown in Fig. 6a.

The intensity errors caused by the movement of the illumination-flat M_2 are negligible because its gradient is very small across the camera field (see Fig. 6b). Thus a shift of even several pixels does not match any measurable effect in intensity changes. We separated the M_2 (together with the shutter-flat M_3) directly in the flat-fielding procedure as the "soft" part of the flat-field matrix M.

The movement of the slit-flat M_5 is much more important. This flat-field is caused by dust and defects of the spectrograph slit. These show rapid changes of the intensity across the camera field in the Y direction and they are seen as the horizontal white and black lines and stripes described in Fig. 2 and mentioned above many times. The movement of the slit-flat M_5 acts in both the X and Y direction in the spectrum.

The movement of the slit-flat M_5 in the X direction is not important. The horizontal lines do not significantly change their intensities in the X direction because the inclination of the image was corrected in the previous step of the reduction (cf. Sect. 4.4.1).

But movement of the slit-flat M_5 in the Y direction by even a fraction of a pixel changes dramatically the whole "hard" flat-field matrix $M_{1,4,5}$ which then does not match the conditions valid for the observed spectrum S_2. To solve this problem, one has to separate the slit-flat M_5 from the "hard" part of the flat-field matrix $M_{1,4,5}$ (Fig. 6a), to be able to shift only the slit-flat M_5 in the Y direction, to fit the particular spectrum S_2 well.

Separation of the slit-flat M_5

We benefited from the fact that only the slit-flat M_5 is uniform in the X direction. This is a direct consequence of the imaging of the slit on the focal plane of the spectrograph. Thus, the vector made as an average of all columns of the "hard" flat-field $M_{1,4,5}$ will mainly represent the fluctuations of the slit-flat M_5 in the Y direction because the other two components, the pixel-flat M_1 and the camera-flat M_4, are randomly distributed across the CCD image and they will not contribute systematically to the averaged vector. We denoted this vector the "slit-vector" (see Fig. 7). We created a new array of the same dimensions as the spectrum S_2 and the "slit-vector" was replicated in all columns of the created array. Thus, this new array represents the pure slit-flat M_5 (see Fig. 6c). Obtaining the pure slit-flat M_5 makes it possible to extract the pixel-flat and the camera-flat $M_{1,4}$ dividing the "hard" flat-field matrix $M_{1,4,5}$ by the pure slit-flat M_5. The resulting $M_{1,4}$ is shown in Fig. 6d.

4.5. Flat-fielding

At the beginning of Sect. 4 we defined the *simple, extended* and *precise* reductions. According to those definitions, we can rewrite Eq. (3) valid for flat-fielding in the three following forms:

Simple flat-fielding

This flat-fielding was done with the flat-field matrix $M_{1,2,3,4,5}$ which was constructed according to Eq. (10) directly from the raw mean flat-field frame F_{mean} (cf. Fig. 2) corrected only for the segment-flat M_6. So the simply reduced spectrum R_1 is defined by the equation:

$$R_1 = S_1 \frac{1}{M_6} \prod_{i=1}^{5} \frac{1}{M_i}, \tag{11}$$

where the spectrum S_1 defined by Eq. (6) was corrected for background and different sensitivities of the segments of the CCD chip only. The *simple* spectral characteristics were calculated using this reduced spectrum R_1.

Extended flat-fielding

In the *extended* approach of the flat-fielding we omitted only step 4.5 of the reduction, i.e. the appropriate shift of the slit-flat matrix M_5. The consequence is that the flat-field matrix M exhibits a shift comparing to the spectrum S_2. Thus, the equation used for *extended* flat-fielding is formally identical to the previous one:

$$R_2 = S_2 \frac{1}{M_6} \prod_{i=1}^{5} \frac{1}{M_i}, \tag{12}$$

but the spectrum S_2 represents here the manipulated prepared spectrum S_2 shown in Fig. 5a, and the flat-field matrix $M_{1,2,3,4,5}$ was retrieved from the prepared mean flat-field frame F_{mean} shown in Fig. 5b. It means that S_2 as well as F_{mean} were corrected not only for background and different sensitivities of the segments of the CCD chip but also for the X inclination of the image and for stretching and the Y inclination of the spectral lines. The resulting R_2 is shown in Fig. 8a.

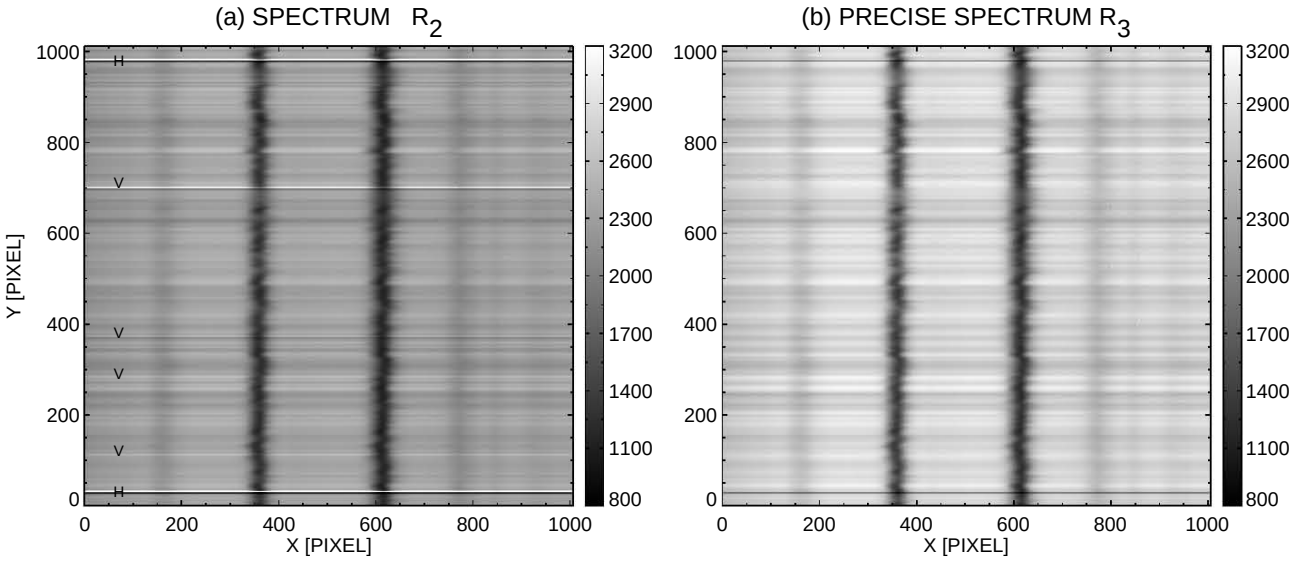

Fig. 8. a) The spectrum R_2 as the resultant of the *extended* reduction made according to Eq. (12). The symbols V and H denote the sharp intensity spikes resulting from incorrect fitting of the strips and lines caused by dust and defects on the spectrograph slit and by the artificial wires seen in the prepared spectrum S_2; **b)** The spectrum R_3 as the resultant of the *precise* reduction made according to the Eq. (13). The grey-scale bars give relative intensities expressed in ADU.

Table 2. Mean signal $\overline{Si}$ (ADU) and standard deviations "STD" of the original and reduced arrays.

	P Fig. 1	$P - G_{\mathrm{mean}}$	R_1	R_2 Fig. 8a	R_3 Fig. 8b
$\overline{Si}$	2192	2149	2308	2291	2282
STD [%]	5.61	5.72	5.67	6.09	4.72

P = raw spectrum, G_{mean} = mean background, R_1 = "simple" spectrum, R_2 = "extended" spectrum, R_3 = "precise" spectrum.

The *extended* spectral characteristics were calculated using this reduced spectrum R_2. There are still sharp horizontal lines and stripes in R_2. This is due to temporal changes of the flat-field conditions mainly caused by the drift of the spectrograph. Thus, the mean flat-field frame F_{mean} constructed from the flat-field source frames F taken at the beginning of the observing run does not perfectly match the flat-field conditions valid for the moment of the particular spectrum P registration. The resulting flat-field matrix $M_{1,2,3,4,5}$ is slightly shifted in both directions comparing to S_2. So, some defects are enhanced instead of suppressed in R_2.

Precise flat-fielding

To avoid the consequences mentioned above the *precise* flat-fielding differs in the following way: we compared the "Y" coordinates of the WL wires in the slit-flat M_5 (Fig. 6c) and in the prepared spectrum S_2 (Fig. 5a) looking for the highest correlation. The difference and direction in which the slit-flat M_5 must be shifted in the Y direction to fit the prepared spectrum S_2 was found. For the shift of the slit-flat M_5 we used our procedure in which the image is re-binned 100 times up to get a shift accuracy of 1/100 of pixel. This was done step by step, along the X direction to avoid the production of an extremely large array. It means that every particular column of the image was re-binned 100 times, shifted appropriately and re-binned back. The Eq. (12) will be modified in this case to equation:

$$R_3 = S_2 \, \frac{1}{M_6} \prod_{i=1}^{4} \frac{1}{M_i} \, \frac{1}{M_5}\,, \tag{13}$$

where the S_2, M_6 and M_i are identical to those which take place in Eq. (12) and M_5 denotes the new shifted slit-flat M_5. The precise spectrum R_3 reduced according to Eq. (13) is represented in Fig. 8b.

We need to keep the positions of the artificial wires WL for adjustment between the two CCD images taken with different CCD cameras in different spectral regions. Therefore, just before dividing the prepared spectrum S_2 by the flat-field matrices, the central rows of the artificial wires WL in the flat-field matrices were replaced by rows of mean intensity. After dividing the spectrum by the flat-field matrices the two horizontal central WL wires appeared back in identical positions in the reduced spectrum R_3 because they had not been removed from the prepared spectrum S_2.

5. Results

The reduction of the solar spectra should improve the S/N ratio in the spectra but on the other hand the shape of the spectral lines must be not affected. Therefore we tested both the noise propagation through the data and analysis of corrupting of the shape of the spectral lines. First, the standard deviations of different types of arrays were computed and secondly, the

Table 3. Mean signal $\overline{Si}$ (ADU) and standard deviations "STD" of the measured arrays.

	G	G_{mean} Fig. 3	F	$F-G$	$F-G_{\mathrm{mean}}$	F_{mean} (1) Fig. 2	F_{mean} (2) Fig. 5b	$M_{1,4,5}$ Fig. 6a	$M_{2,3}$ Fig. 6b	M_5 Fig. 6c	$M_{1,4}$ Fig. 6d
$\overline{Si}$	44	44	1248	1204	1204	1205	1303	1	1	1	1
STD [%]	2.87	0.80	4.96	5.06	5.04	5.09	4.84	2.59	1.44	2.27	1.23

G = background, G_{mean} = meanbackground, F = flatframe, $F_{\mathrm{mean}}(1)$ = rawmeanflat, $F_{\mathrm{mean}}(2)$ = preparedmeanflat, $M_{1,4,5}$ = "hard" part of M, $M_{2,3}$ = "soft" part of M, M_5 = slit-flat, $M_{1,4}$ = pixel and camera flat.

accuracy of the spectral characteristics determined from the *simple, extended* and *precise* reductions was examined.

5.1. Standard deviations

Generally noisy data have a higher standard deviation of the signal then the good data. This is not the case for the solar spectra. One must distinguish between the noise coming from defects and noisy flats and between the real physical variations of the intensity across the image. For example the best solar spectra of the solar granulation reach a standard deviation of the intensity variation along the slit between 6%–7% after reduction. Therefore, it is important to analyze if the standard deviation was decreased by the reduction process and not to be afraid of the big standard deviation of the resulting spectra.

The standard deviations of the signal of the original as well as of the reduced spectra are given in Table 2 and the standard deviation of the signal of the "supporting" arrays (G, F, M) are shown in Table 3. We estimated the standard deviations only from a limited area of any spectral array, to exclude the contribution of the spectral lines to the values. An area was selected in the upper right corner of the arrays, marked by the rectangular box in the array in Fig. 5. Because of the absence of spectral lines in the flat-field matrix M the calculation of the standard deviations in these arrays (the last four column in Table 3) was done in the whole area between the wires WL. We will discuss these results in Sect. 6.

5.2. Spectral characteristics

The stability of the shape of the spectral lines was tested using spectral characteristics of the spectra R_k, $k = 1, 2, 3$ resulting from the *simple, extended* and *precise* reduction respectively. Only 946 scans selected between the WL wires were used for the analysis.

Several manipulations were applied to every scan of the R_k before the spectral characteristics were calculated:
a) the local continuum of every scan was determined on the left and right side of the spectral line as a maximum of the second order polynomial fit of selected intervals of intensities. Because of the very small spectral region recorded on the CCD chip (no true continuum level available beside the lines), these intervals are not the 100% continua valid for this spectral region. They could be recalculated to the true continua using the solar spectrum atlas. The intensity of the "quasi-continuum" interval available beside the lines in the spectrum is compared with the intensity of the same interval available in the solar atlas. The ratio between them serves for correction. But for our purpose, to compare the relative difference of spectral characteristics, this was not necessary;
b) Fast Fourier Transform was used for high frequency signal filtering to smooth data of every scan. Optional Gaussian filtering of high frequency noise (cf. Gray 1992) has effectively filtered all power above 1/10 of the Nyquist frequency;
c) the zero position for determination of shifts of line centres and bisectors was calculated as the position of the centre of the mean profile. The mean profile was constructed as an average of the 946 profiles;
d) a spectral line inclination in R_1 which resulted from the *simple* flat-fielding was eliminated, i.e. we applied de-stretching after the flat-fielding in this case.

The spectral characteristics, continuum intensity (I_{c}), line centre intensity (I_{o}), line Doppler shift (L_{sh}), bisectors Bi and full width at half maximum (*FWHM*) were calculated separately for every scan for all three types of resulting spectra R_{k}. In Fig. 9 the line center intensity fluctuations I_{o} along the slit (Y direction) resulting from *precise*, *extended* and *simple* reduction are shown. For comparison of the results we used the differences of the spectral characteristics. We use the results given by the *precise* flat-fielding as a standard for the estimation of the relative errors of the values resulting from the other two reduction approaches. The relative differences of the line centre intensities $RD_{3,i}$, $(i = 1, 2)$ expressed as a percentage were calculated as:

$$RD_{3,i} = \frac{I_{\mathrm{o}3} - I_{\mathrm{o}i}}{I_{\mathrm{o}3}} * 100., \quad i = 1, 2, \tag{14}$$

and the mean of the result was normalized to a value of 0.0. The relative differences of I_{c} and of *FWHM* were calculated in the same way. The results are shown in Fig. 10.

The absolute differences of the line centre shifts $AD_{3,i}$, $(i = 1, 2)$ expressed in $\mathrm{m\,s^{-1}}$ were calculated according to the equation:

$$AD_{3,i} = L_{\mathrm{sh}3} - L_{\mathrm{sh}i}\,, \quad i = 1, 2\,, \tag{15}$$

where $L_{\mathrm{sh}3}$ denotes the line shifts resulting from *precise* flat-fielding (spectrum R_3), and $L_{\mathrm{sh}1}$ and $L_{\mathrm{sh}2}$ denote the line centre shifts resulting from *simple* flat-fielding (spectrum R_1) and from *extended* flat-fielding (spectrum R_2), respectively. The results are shown in Fig. 11.

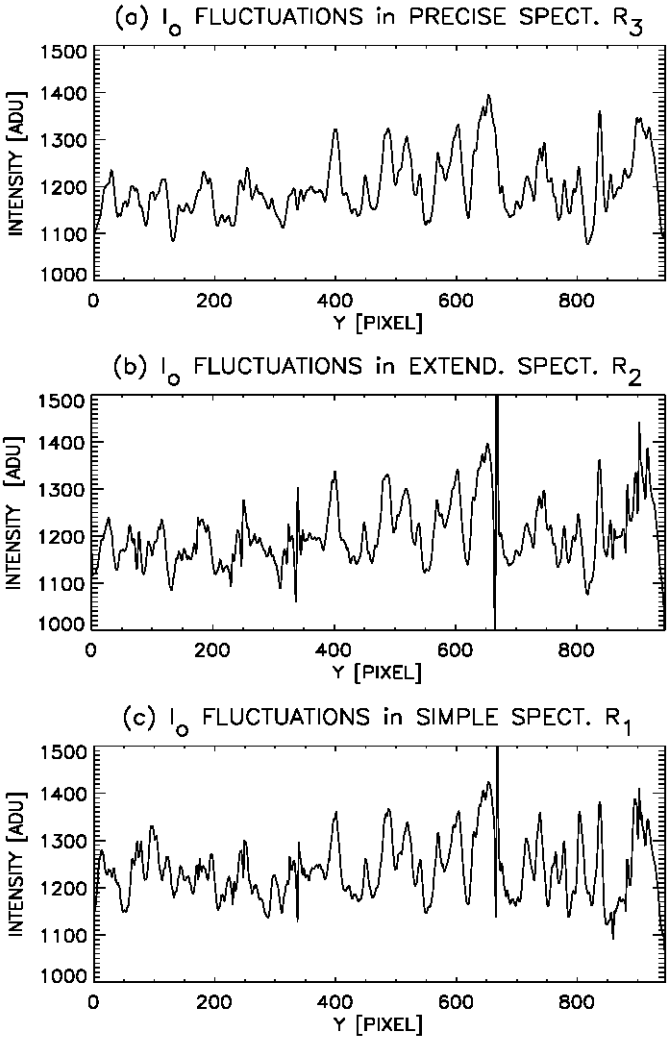

Fig. 9. Line centre intensity fluctuations I_o along the slit (Y direction) resulting from: **a)** *precise*, **b)** *extended* and **c)** *simple* flat-fielding. The difference of the first and third panel is shown in Fig. 10b and the difference of the first and second panel is shown in Fig. 10e.

The absolute differences of bisectors Bi were calculated in the same way as for the line shifts and the results for bisectors at 0.2, 0.4, and 0.6 of the line intensity are shown in Fig. 12.

6. Discussion

The precise reduction applied on the raw spectrum P significantly decreased the noisy signal coming from the flat-field. The relative standard deviation of the signal of the raw spectrum P was 5.61% (see Table 2) and the resulting spectrum R_3 had a relative standard deviation of 4.72%. Although the last number seems to be rather big the variations of the signal in the resulting spectrum R_3 are caused by real physical variations of the solar granulation. The other numbers given in Table 2 documented that both the *simple* reduction (spectrum R_1) and the *extended* reduction did not help to minimize the noise in the raw spectrum P. The *simple* spectrum R_1 shows a smaller standard deviation of the signal than the spectrum R_2 but the shapes of the spectral lines in the spectrum R_1 were affected. The signal of the reduced spectra is higher comparing to the raw observed spectrum P due to correction of the spectrum by segment-flat M_6.

We have also analyzed the degradation of the signal in the spectra, caused by different types of flat-fields and by the background. Table 3 clearly shows that an averaging of only 7 background images G suppressed the noise in the mean background G_{mean} significantly. On the other hand no significant difference of the standard deviation is seen in all flat field frames but they all have smaller noise than the raw spectrum P due to their "flat" character.

The contribution of the different components of the flat-field matrix M to the noise of the original raw spectrum P is documented by the last four columns of the Table 3. The "hard" part $M_{1,4,5}$ is more significant in this way ($STD = 2.59\%$) than the "soft" part $M_{2,3}$ with a standard deviation of 1.44%. More, the main contributor to the noise of the flat-field matrix $M_{1,4,5}$ is the slit-flat M_5 as can be seen in the two last columns of the Table 3. The standard deviation of M_5 is roughly two times higher compared to the pixel and camera flats $M_{1,4}$. This clearly documents that the slit-flat M_5 plays an important role in the flat-fielding of the solar spectra.

b) spectral characteristics

Spectral characteristics determined from spectra reduced with different accuracy exhibit significant differences. The widely used *simple* approach of reduction, produced fully insufficient accuracy of the results. The most influenced were the central parts of the spectral lines as a consequence of applying of an incorrect flat-field matrix $M_{2,3}$ i.e. the illumination-flat and shutter-flat (see Fig. 4a). Significant errors for line centre intensities I_o and for full width at half of line maxima $FWHM$ are documented in this case. Only a small fraction of the data has accuracy better than 3% (see the part of 400–600 pixel in Figs. 10a,b). The relative errors of the rest of the data fluctuate by up to 10%. The humps of data in these two panels are caused by insufficient correction of the curvature of the spectral lines in the *simple* reduction. Only the central parts of the image are sufficiently corrected using the flat-field matrix $M_{2,3}$ (cf. Fig. 4). Then the difference between the correct data derived from *precise* reduction and the data resulting from the *simple* reduction shows humps.

In the *simple* case the continuum intensities I_c were less influenced: they differ from the *precise* values by 1%–2%. Several values exceeded 3%. These excesses appeared at those positions where the intensity of the original raw spectrum P was strongly reduced by dust particles on the slit.

The differences of line centre Doppler shifts L_{sh} are also significant. They exceeded 200 $\mathrm{m\,s^{-1}}$ (cf. Fig. 11a). The L_{sh} measured in the *precisely* reduced spectrum reached $\sim$1 $\mathrm{km\,s^{-1}}$. Thus a velocity of 200 $\mathrm{m\,s^{-1}}$ represents an error of $\sim$20%. Similar results were found for bisectors (cf. Figs. 12a–c).

The *extended* reduction improved the results slightly but still not sufficiently. The relative differences of I_c as well as of I_o (cf. Figs. 11d,e) remain under 1% except those cases when the intensity of the original raw spectrum was reduced by dust particles on the slit. In this case the relative differences of I_c as

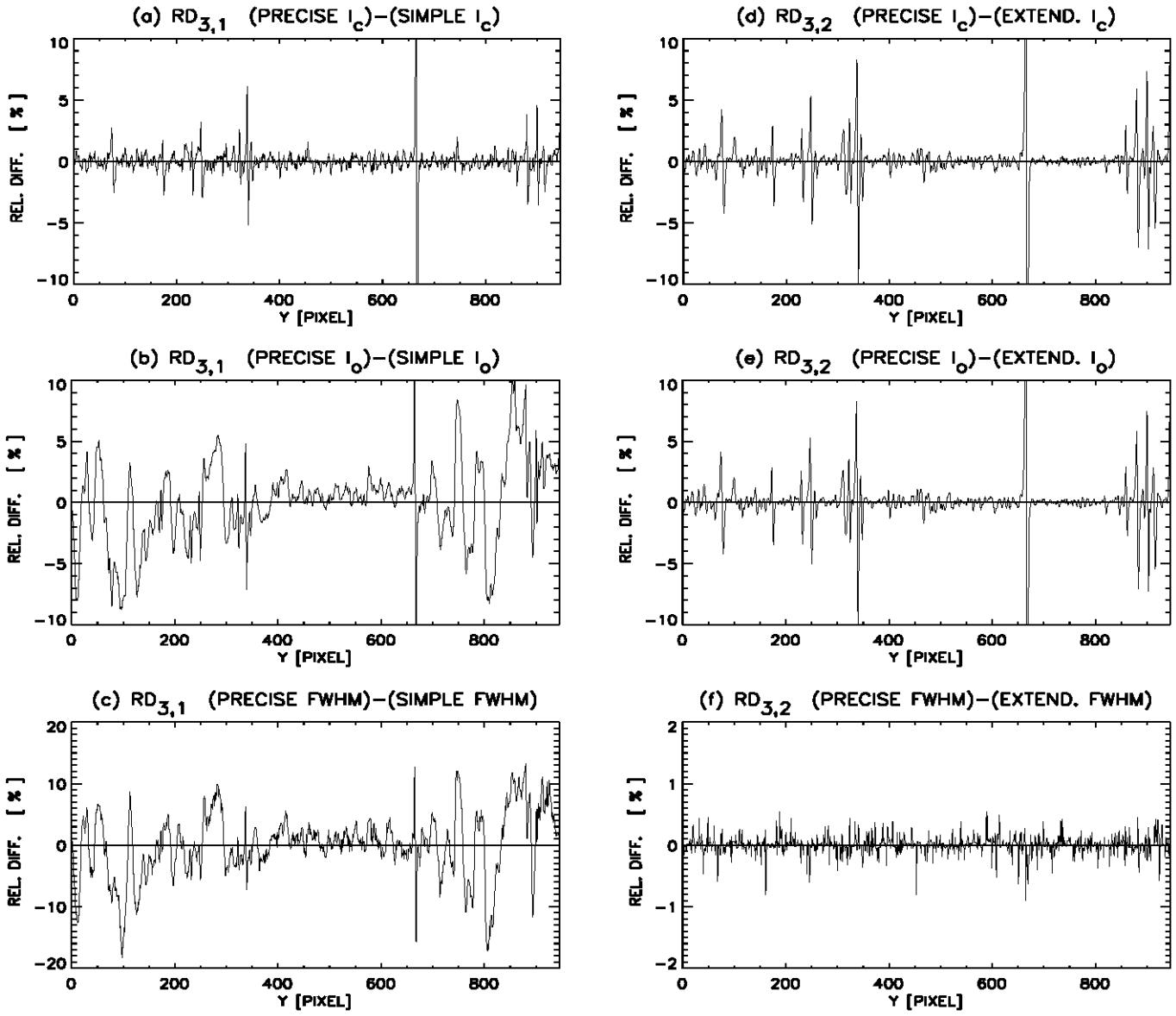

Fig. 10. The relative differences $RD_{3,1}$ of (*precise – simple*) results **a–c)** and relative differences $RD_{3,2}$ of (*precise – extended*) results **d–f)** calculated for continuum intensity (I_c), line centre intensity (I_o) and full width at half maximum (*FWHM*) according to Eq. (14). Notice the scaling of factor 10 between the graphs of *FWHM*.

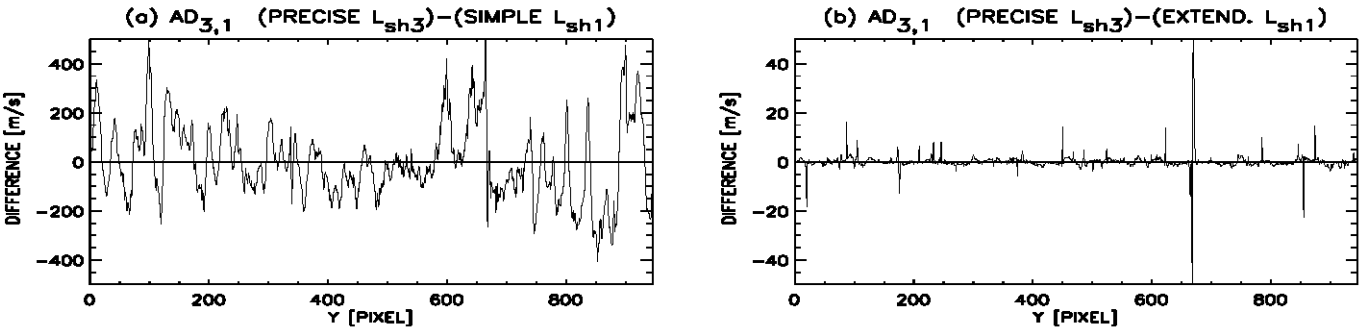

Fig. 11. Absolute differences of line centre shifts L_{sh} expressed in m s^{-1}, calculated according to Eq. (15). **a)** Difference between *precise* and *simple* flat-fielding; **b)** difference between *precise* and *extended* flat-fielding.

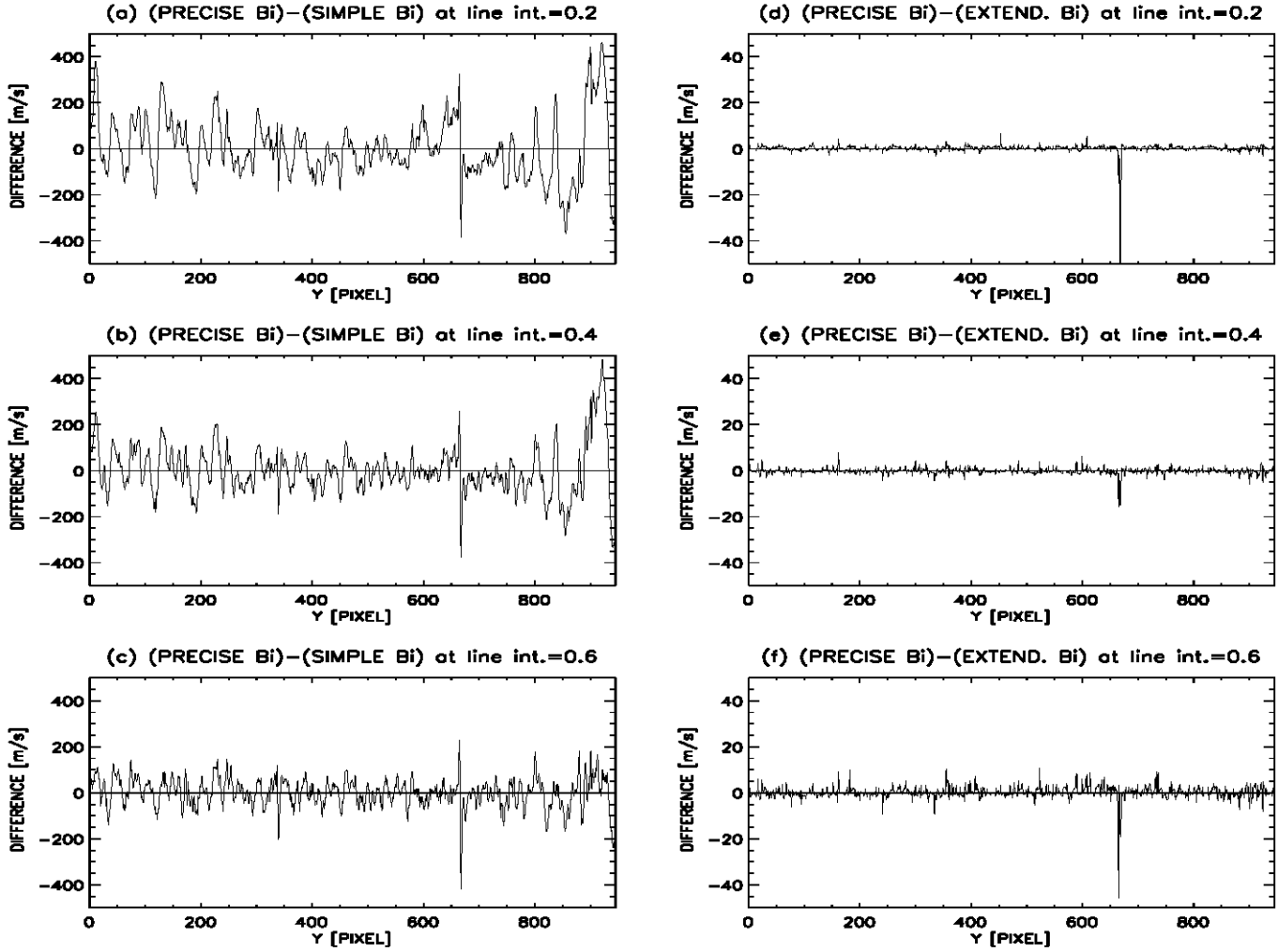

Fig. 12. Absolute differences of bisectors Bi expressed in $\mathrm{m\,s^{-1}}$, calculated using the Eq. (15). **a)** Difference between *precise* and *simple* flat-fielding; **b)** difference between *precise* and *extended* flat-fielding. The panels from the top represent calculations for bisectors determined at 0.2, 0.4 and 0.6 of the line intensity respectively.

well as of I_o exceeded 2% and some "spikes" reached 5% and more.

Almost identical values of *FWHM* resulting from the *extended* and from the *precise* reductions were found. The differences of the *FWHM* were less than 0.2%. Only a few values exceeded 0.5%, again at those positions where the wires imposed by dust on the slit appeared in the original raw spectrum.

Similarly to the *FWHM* case, the line centre Doppler shifts L_{sh} were also not very sensitive to the temporal changes of the flat-field conditions. The differences of L_{sh} were smaller than 3 $\mathrm{m\,s^{-1}}$ and only a few values reached 10 $\mathrm{m\,s^{-1}}$ (cf. Figs. 12d–f). The relative errors of this data are of 0.3%–1.0%.

The small sensitivity of the *FWHM* and L_{sh} to the change of flat-field conditions can be explained by the fact that the shift of the slit-flat M_5 did not significantly change the position and the shape of the particular line profile but it mostly changed the intensity of the line and of the continuum. This fact is also documented by the differences of bisectors which gradually increased at higher intensities of the spectral line (cf. Figs. 12d–f). The differences of bisectors at a line intensity 0.2 were smaller than 2 $\mathrm{m\,s^{-1}}$ and gradually increased up to 10 $\mathrm{m\,s^{-1}}$ for bisectors calculated at line intensity of 0.8 (not shown in figure). The relative errors in all these cases fluctuated between 0.2%–1.0%.

In the case of the *simple* reduction, the accuracy of the determination of the bisectors increased gradually when the bisectors were calculated for higher positions of line intensity. An opposite trend in the case of the *extended* reduction was found, but the accuracy of this approach was still one and half times better than in the *simple* reduction.

7. Conclusions

Using the precise procedure suitable for reduction of large solar CCD spectra and comparing the *simple* and *precise* approaches of the reduction we documented:

1) It is essential to apply de-stretching (i.e. correction of the curvature and inclination of the spectral lines) before flat-fielding instead of after it, since the determined spectral line characteristics will have significant errors.

2) Only the precise reduction sufficiently suppresses the noise coming from the various components of the flat-field matrix M.

3) The most noisy component of the raw spectrum is the flat-field caused by the defects of the slit and by dust on the slit of the spectrograph.

4) Splitting of the flat-field matrix into several components and appropriate shifts of them should be applied in the case when the flat-field conditions were significantly changed during the observing run. In particular, this should be applied if the particular spectrum was taken much later than the flat-field frames.

5) The continuum intensities and line centre intensities are the spectral characteristics most sensitive to the temporal changes in the flat-field conditions.

6) Precise flat-fielding is essential for correct reduction of the large solar CCD spectra, because the inaccuracy remaining from insufficient reduction approaches will still affect all results based on the analysis of the profiles of spectral lines.

Acknowledgements. The VTT is operated by the Kiepenheuer-Institut für Sonnenphysik, Freiburg, at the Observatorio del Teide of the Instituto de Astrofisica de Canarias. Part of this work was supported by the Slovak grant VEGA 2/7229/20 and German DFG grant No. 436 SLK 113/7. A.H., A.K. and J.R. thank the Austrian and Slovak Academies of Sciences for financing the exchange of scientists. A.H. acknowledges the support of the Austrian Fond zu Förderung der wissenschaftlichen Forschung (No. 13308). We would like to thank H. Schleicher for the programs made for the IDL KIS LIB.

References

Balthasar, H., Thiele, U., & Wöhl, H. 1982, A&A, 114, 357
Beletic, J., & Amico, P. 1998, Astrophys. Space Sci. Libr., 228
Brault, J. 1979, Osservazioni e Memorie dell'Osservatorio Astrofosico di Arcetri, 106, 33
Gray, D. F. 1992, The Observations and Analysis of Stellar Atmospheres (Cambridge Univ. Press),
Harrison, P. J. 1999, Amer. Astron. Soc. Meet., 194, 76.12 (American Astronomical Society)
Holst, G. C. 1998, CCD arrays, cameras and displays, 2nd edition (JCD publishing and SPIE Optical Engineering Press, USA)
Johanneson, A., Bida, T., Lites, B., & Scharmer, G. B. 1992, A&A, 258, 572
Kentischer, T., & Schleicher, H. 1997, private comunication
Kuhn, J., Rimmele, T., & Stauffer, F. 1997, NOAO Newsletter, National Solar Observatory, March 1997, No. 49
Martinez, P., & Klotz, A. 1998, A practical guide to CCD astronomy (Cambridge University Press, Practical Astronomy Handbooks), No. 8
Newberry, M. V. 1991, Pub. Astron. Soc. Pacific, 103, 122
Newberry, M. V. 1999, Precision CCD Photometry, ASP Conf. Ser., 189, 74
Schröter, E. H., Soltau, D., & Wiehr, E. 1985, Vistas Astron., 28, 519
Thiele, U. 1982, Diploma-thesis (in German), University of Göttingen